Heliyon 9 (2023) e20665

Contents lists available at ScienceDirect

Heliyon

journal homepage: www.cell.com/heliyon

Adsorption characteristics of magnetized biochar derived from *Citrus limetta* peels

Ayushi Mishra [a], Himanshu Ojha [b], Jyoti Pandey [a,**], Anjani Kumar Tiwari [a], Mallika Pathak [c,*]

[a] *Department of Chemistry, Babasaheb Bhimrao Ambedkar University, Lucknow, 226025, Uttar Pradesh, India*
[b] *Division of Radiological, Nuclear and Imaging Sciences, Institute of Nuclear Medicine and Allied Sciences, Brig S K Mazumdar Road, Timarpur, Delhi, 110054, India*
[c] *Department of Chemistry, Miranda House, University of Delhi, Delhi, 110007, India*

ARTICLE INFO

Keywords:
Biochar
Adsorption
Wastewater remediation

ABSTRACT

Agro-industrial waste is an alarming issue that needs to be addressed. Waste valorization is an effective technique to deal with such effectively. Synthesis of biochar from fruit waste is one of the emerging approaches for adsorption, energy storage, air purification, catalysis, and biogas production trending these days. Magnetized *Citrus limetta* biochar (MCLB) was synthesized from *Citrus limetta* peels and was magnetized using iron oxide. Magnetization of biochar increases its functionalities as well as makes its separation easy. The removal of Methylene Blue (MB) dye from an aqueous solution is achieved through the use of MCLB. Methylene Blue is a prominent and widely used cationic-azo dye in the textile and printing industries. The accumulation of MB in wastewater is the major problem as MB is reported as a carcinogenic agent. The removal of MB dye with MCLB was analyzed by adsorption studies, wherein the effect of factors influencing adsorption such as initial concentration of MB dye, MCLB dosage, the effect of pH, contact time, and adsorption isotherms were studied. Characterization of MCLB was carried out using various techniques, such as FTIR, VSM, XRD, SEM, RAMAN, and Zeta potential. The adsorption isotherm mechanism was well explained with the non-linear Langmuir isotherm model resulting in a good adsorption capacity (q_e = 41.57 mg/g) of MCLB when MB (c_o = 60 mg/L, pH ~ 6.8, T = 273K). The thermodynamics analysis revealed that MB's spontaneous and endothermic adsorption onto the MCLB surface followed pseudo-second-order kinetics. The results obtained from this study suggest that the magnetized biochar derived from *Citrus limetta* peels has a wide range of potential applications in the treatment of dyeing wastewater.

1. Introduction

There has been an upsurge in demand over the last few years for sustainable solutions to environmental issues [1]. The environment and human health are at threat from industrial wastewater effluents that have not been correctly treated such as leather, textiles, cosmetics, paint, food packaging, pharmaceuticals, paper printing, and personal care products (PCPPs) [2]. It is common knowledge

* Corresponding author. Department of Chemistry, Miranda House, University of Delhi, Delhi, 110007, India.
** Corresponding author. Department of Chemistry, Babasaheb Bhimrao Ambedkar University, Lucknow, 226025, Uttar Pradesh, India.
E-mail addresses: jyotipandey@bbau.ac.in (J. Pandey), mallika.pathak@mirandahouse.ac.in (M. Pathak).

https://doi.org/10.1016/j.heliyon.2023.e20665
Received 10 May 2023; Received in revised form 22 September 2023; Accepted 3 October 2023

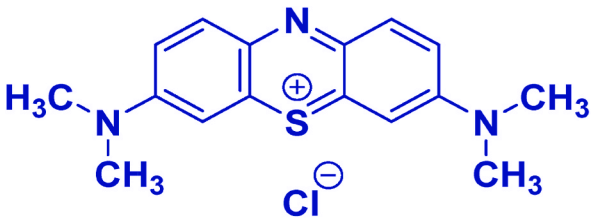

Fig. 1. Structure of methylene blue (M.W. = 319.85 g/mol)

that dyeing and finishing processes in the textile industry result in effluents including surfactants, color, dissolved solids, and some amount of heavy metals ions [3]. Presently, India ranks as the sixth-largest manufacturer of textiles and apparel globally. (https://texmin.nic.in/sites/default/files/AR_Ministry_of_Textiles_%202021-22_Eng.pdf). Around 1000 L of water is used in the dyeing process for every 1000 kg of treated fabric. Such dye discharge colors the receiving water bodies (lakes and rivers), making it difficult to utilize them for their intended purposes [4]. In the aforementioned industries, the use of dyes to add color produces a lot of effluents, which are hazardous to human health and the environment. Dye removal is necessary to stop the emission of effluents into the environment [5]. In general, dyes can be classified into cationic and anionic groups according to the chemical nature of those groups. A common cationic dye known as methylene blue (MB) Fig. 1 is released in large amounts into natural water sources by the textile industry, endangering both human health and the environment.

From an environmental standpoint, Synthetic dyes must be eliminated since some of the dyes and the byproducts of their breakdown may be dangerous and carcinogenic, therefore their treatment cannot be completely dependent on bio-degradation [6].

Many treatment techniques, which include membrane via separation, enzymatic decolorization adsorption, ion exchange, chemical precipitation, ultrafiltration, and sedimentation, are used to remove MB from the water [7,8]. Nowadays, adsorption technology using affordable adsorbents has emerged as a primary method of removing MB, and A number of researchers are studying that method [9,10]. Biochar has quite popular because of its special capabilities to remove contaminants from water and lower manufacturing cost among adsorbents.

According to research, adsorption is a common method for removing both inorganic and organic chemical pollutants. According to the majority view, adsorption is a better alternative processing technique in cost-effectiveness, ease of use, versatility, and sensitivity to toxic contaminants [11]. Collectively, chemical adsorption and physical adsorption are effective to create the adsorption process. Physical adsorption, which frequently takes place at lower temperature bleaching operations, depends on intermolecular interactions between the pollutant's and the adsorbent's surface groups to create selective combined single and multilayer adsorption that requires less activation energy. Chemical adsorption is frequently involved in high-temperature processes. The asymmetry of the gravitational pull on the adsorbent's surface is caused by the unequal distribution of its atoms, and as a result, the adsorption of specific compounds has an impact on the free energy of the surface molecules. To generate shared electrons or transmit electrons between adsorbates, monolayer, selective adsorption is employed [12]. The adsorption of synthetic dyes on affordable and effective solid supports such as Clay, activated carbon, silica, graphene oxide, zeolites, and biochar was thought to be an easy and affordable way for their removal from water and wastewater as conventional techniques cannot efficiently remove synthetic dyes from wastewater [11]. Food waste and agroindustrial waste are significant worldwide issues. Globally, more than each year, approximately 1 billion metric tons of food waste is discarded, and billions of people are involved in the entire food supply chain. The carbon value of these waste sources is beneficial and is similar to the annual use of all chemicals and polymers with the benefit that the former is renewable, which makes it astonishing [13]. Activated carbon, unconventional low-cost adsorbents, some naturally occurring materials like clay, biomass (dead and living), zeolites and other siliceous materials, waste products, and by-products from Industrial and agricultural waste (Agricultural solid wastes & Industrial solid wastes), and other adsorbents are used thermochemical procedures such as sewage sludge, wood husks, animal and poultry manure, agricultural straw, and other solid wastes to create biochar. Citrus fruits are the most commonly traded fruits globally, and India holds the sixth position in terms of citrus fruit production worldwide. The world's tropical and subtropical areas produce more than 120 million tonnes of citrus each year. About ≈40–60% of the fruit is non-edible and gets discarded as waste [14]. Millions of tonnes of by-products like fruit peels and seeds are produced by the fruit processing industries, and their disposal poses a threat to the environment. Depending on their disposal, food waste of both vegetable and fruit origin poses an imminent threat to the environment in the 21st century. The majority of India's food processing businesses are micro and small-scale industries that lack resources including funding, workspace, technology, and expertise in making the utilization of by-products. In developing countries like India, the average cost of transport was found to be between $11 and $15 per tonne for each trip. (FICCI, 2010), which may represent a total cost of >$300 million for landfilling food waste [15]. According to the United Nations Environment Programme (UNEP), 121 kg of food is wasted globally per person each year, and 74 kg of food waste is generated in households. Waste management faces financial and logistical strain because it is challenging to decompose food waste [16]. Fruit and vegetable waste are expected to equal 12 and 21 million tonnes or around 4.4 billion USD, with a total food worth loss and waste processed of 10.6 billion USD, respectively, according to the MFPI (Ministry of Food Processing Industries of India) [17]. Huge amounts of this food waste are burned, disposed of in the nearby river or landfill, or both, which pollutes the ecosystem and lowers the quantity of dissolved oxygen in polluted water [18]. Methane, which contributes to global warming is 28 times more harmful than carbon dioxide and is released as the decomposition of food wastes. Non-consumed foods are responsible for 8–10 % of the planet's greenhouse gas (GHG) emissions, according to UN research studies. Carbon footprints reveal that Food waste was the third-largest worldwide Greenhouse gas emitter in

Table 1
Remediation of various dyes by different food waste biochar adsorbents.

S.No.	Adsorbents	Adsorbate	q_{max} (mg/g)	Reference
1.	Litchi peel biochar	Congo red	404.4	[23]
2.	Potato peels (PPc)	Cibacron blue	270.3	[24]
3.	Dragon fruit peels (DFPAC)	Methyelene blue	195.2	[25]
4.	Coconut shell (MACz)	Methylene blue	156.25	[26]
5.	Fava bean peel (FBP)	Methylene blue	140.00	[27]
6.	Moringa oleifera leaves (ACB)	Methylene blue	136.99	[28]
7.	Orange peel (MAB)	Congo red	136	[29]
8.	Banana stem (ACBS)	Methylene blue	101.01	[30]
9.	Crisp Persimmon Peel (CPP-200)	Methylene blue	59.72	[31]
		Alizarin yellow R	4.05	
		Neutral red	39.08	
10.	Tapioca peel (S@TP)	Malachite green	30.18	[32]
		Rhodamine B	33.10	
11.	Litseaglutinosa seeds (ACBs)	Methylene blue	29.03	[33]
12.	Pamelo peel (FO-PPB)	Reactive red 21	26.25	[34]
13.	Mandarin peel biochar ($ZnCl_2$ treated)	Methyl orange	16.27	[35]
		Fast green FCF	12.44	
14.	Black cumin seeds (BCC)	Methylene blue	12.85	[36]
15.	Pineapple fruit peel biochar (PFPB)	Patent Blue	10.29	[37]
16.	Magnetized *Citrus limetta* biochar (MCLB)	Methylene blue	41.57	This study

2019 [19]. To be sustainable, waste must be recycled and repurposed into useful by-products for humankind. Many researchers have worked on the remediation of various dyes by different food waste biochar adsorbents Table 1. Zhang et al., 2018 prepared magnetized biochar (MMABC) by utilizing Melia azedarch wood to remove Cr(IV) ions from aqueous solutions. The researchers found that the maximum adsorption capacity was 25.27 mg/g. Boudraa et al., 2022 developed magnetite-modified orange peel biochar (OPB/Fe_3O_4) as an adsorbent for removing crystal violet dye from aqueous solutions. The researchers found that at 50 °C, the maximum adsorption capacity was 113 mg/g [20].Nguyen et al., 2020 synthesized pomelo peels loaded with Fe_3O_4 nanoparticles (FO-PPB) and employed them as an adsorbate to extract reactive red dye from aqueous solutions. Their adsorbent (FO-PPB 2 g/L) showed a maximum adsorption capacity of 26.25 mg/g. Suhaimi et al., 2022 used locally grown bamboo (Gigantochloa spp.) to synthesize biochar for the adsorptive removal of methylene blue dye. Cheng et al., 2021 synthesized sludge-based biochar (SLAC) for the removal of methyl orange, and the adsorption capacity resulted as 0.8 mmol/g. Srivatsav et al., 2020 concluded in their review that for removing various hazardous dyes from wastewater, biochar is an excellent material. The potential for employing biochar as an adsorbent is enormous.

A stable and carbon-rich substance called biochar may be created from biomass by pyrolyzing it in the absence of oxygen (or with only a minimal amount). Moreover, biochar can be synthesized using a variety of common materials [21]. Biochar offers a wide range of uses in wastewater treatment, biogas production, energy storage devices, soil improvement, and environmental remediation, due to its solid structure, significant specific surface area and pore volume, and abundance of active functional groups. To decolorize wastewater and remove dyes, heavy metals, and other inorganic contaminants, Biochar has many applications as a catalyst or sorbent material. Yet, it is possible to make biochar at a fair price by utilizing a range of materials that are readily accessible [22].

In our research, we assess the viability of using fruit waste to manage industrial wastewater contamination. The aim of the present work was to determine the optimal conditions for the adsorptive removal of Methylene Blue dye, using Magnetized *Citrus limetta* Biochar (MCLB). The current study set out to determine the initial dye concentration of MB, ideal sorbent dose of MCLB, pH of the solution, temperature values, contact time, and initial dye concentration. To further our understanding of equilibrium characteristics and the mechanism underlying the sorption process, we also analyzed the sorption kinetics, equilibrium, and thermodynamics.

2. Material and methods

2.1. Magnetic biochar preparation

Citrus limetta (Mausambi) peels have been collected from a neighborhood fruit juice store in the New Delhi area, free of cost because it was a waste for the shopkeeper. To remove dirt and other water-soluble contaminants, the peels were washed multiple times with distilled water, and then it was sundried for 2–3 days. Before calcination peels were dried in the oven for 24 h at 80 °C. Peels were milled to prepare biomass. The biomass was then carbonized with a heating rate of 5 °C/min for 1 h at 350 °C temperature in Muffle Furnace (Nabertherm GmbH). After that, distilled water was used to clean the synthesized biochar by centrifugation washing method. To avoid solute-inorganic minerals from releasing from biochar during the dye adsorption, biochar can be washed to eliminate them [38]. And it was overnight oven-dried at 80 °C, and then stored for further modification.

Then magnetization of biochar was done by the co-precipitation method used by Oliveira et al., in 2002. The magnetized biochar composite was synthesized from a heterogeneous mixture (400 mL) of biochar in $FeCl_3$ and $FeSO_4$ (1:2) at 70 °C. 100 mL of 5 Molar NaOH solutions was dropwise added into the solution mixture to increase pH to 12 and the iron (II) hydroxides are precipitated. The amount of biochar was set to obtain a biochar/iron oxide composite (1:1 by weight ratio). Post precipitation, magnetized biochar was separated employing a neodymium magnet and Afterward, it was extensively washed with distilled water until the pH of the filtrate

reached around 7. The resulting material was kept for further experiments after being dried in a 60 °C oven for 3 h [39].

2.2. Batch adsorption experiment

Methylene Blue (MB) in chemical grade is as adsorbate without further purification and was purchased from Sigma Aldrich, USA. The desired concentrations of MB solution (20 mg/L, 40 mg/L, 60 mg/L, 80 mg/L, 100 mg/L, 150 mg/L, and 200 mg/L) were made by diluting the stock solution (1000 mg/L), which was made by combining 1 g of MB with 1000 mL of deionized water. At room temperature (25 °C), a specific amount of MCLB was added to a 20 mL solution of MB, and the mixture was mechanically shaken at 160 rpm.

To study the effect of pH, into six Erlenmeyer flasks (100 mL size) about 20 mL of MB solutions (concentration of 50 mg/L) and 0.01 g of MCLB were added. With the addition of 0.1 N NaOH or HCl, the pH was adjusted to the desired value (between 2, 4, 6, 7, 8, and 10). To reach the equilibrium the Erlenmeyers were sealed and shaken for 3 h at a speed of 160 rpm. Using a neodymium magnet, the solid-liquid separations at various times were achieved. After the equilibrium was achieved the remaining MB concentrations were determined using visible light spectrophotometry (SPECORD250 PLUS, Analytikjena, Germany) at = 664 nm.

In order to investigate the effect of contact time, In a 100 mL Erlenmeyer flask 0.04 g of MCLB was introduced to 40 mL of 10 mg/L MB solution at an unadjusted pH (pH 6.8).

The Erlenmeyer flask was sealed and shaken on a 3D-shaker with a speed of 160 rpm for 5–200 min afterward, the suspended adsorbent was separated with the help of a neodymium magnet, and the remaining solution was assessed for any remaining MB utilizing visible light spectrophotometry. (SPECORD250 PLUS, Analytikjena, Germany) at = 664 nm.

To calculate the adsorption capacity of MCLB, in a series of 100 mL Erlenmeyer flasks, 20 mL of MB solutions (concentration of 25–300 mg/L) were prepared and 0.01 g of MCLB is added. The pH of the solutions was unadjusted (pH ≈ 6.8). The sealed Erlenmeyer flasks were shaken with a speed of 160 rpm for 3 h on a 3D shaker. Further, the residual MB concentration was analyzed using visible light spectrophotometry (SPECORD250 PLUS, Analytikjena, Germany) at = 664 nm.

Using equations (1) and (2) the removal efficiency (R, %) and adsorbing capacity (q_e, mg/g) were calculated respectively:

$$R\% = \frac{(C_0 - C_e)}{C_0} \text{ X } 100 \tag{1}$$

$$q_e = (C_0 - C_e)V / m \tag{2}$$

where, V, the solution volume, L; m, the mass of adsorbent, g; C_0 and C_e denoted initial and equilibrium concentrations of MB, mg/L, respectively. The magnetically separated magnetized biochar after adsorption was further oven dried for 12 h at 100 °C and collected to perform further characterizations [40].

2.3. Structural characterizations of MCLB

A SPECORD250 PLUS spectrophotometer (Analytik Jena, Germany) was used to scan the UV–vis absorption spectra of MB throughout the wavelength range of 400–800 nm at room temperature. The Labram HR RAMAN spectrophotometer (HORIBA Scientific) was employed at room temperature to record the Raman spectra of MCLB. Using Cu−Kα 1.54 A^0 radiation and the X Pert-Pro PMRD (D8 Discoverer Bruker AXS, Germany) instrument operated at 40 kV and 30 mA, the X-ray diffraction pattern of MCLB was obtained by preparing a pellet of pure MCLB. MCLB that had been synthesized had its surface morphology analyzed with the SEM (ZEISS SUPRATM 55) instrument. The saturated magnetism of MCLB was obtained at room temperature using a VSM instrument (Microsense, Model ADE-EV9). Fourier transform infrared spectroscopy (FT-IR) was conducted using the KBr pellet method was used in the wavelength range of 400–4000 cm^{-1} (Nicolet iS5, Thermo Fisher, USA).

2.4. Adsorption kinetics

An initial MB concentration of 10 mg/L at an unadjusted pH (pH ≈ 6.8) and a temperature of 303K were employed to perform the kinetic studies. To determine the time required to attain adsorption equilibrium, the solution was shaken on a 3D shaker. The residual concentration of MB was measured by analyzing the absorption intensity of the MB solution with a UV–vis spectrophotometer at defined time intervals (0–4 h). The pseudo-first-order and pseudo-second-order rate equations were used to investigate the mechanism of adsorption kinetics. The equilibrium data were analyzed using the non-linear pseudo-first-order and pseudo-second-order kinetic equations to investigate the mechanism of the adsorption process.

Equations (3) and (4), respectively, represent the non-linear form of pseudo-first-order and pseudo-second-order kinetic equations;

$$q_t = q_e\left(1 - e^{-k_1 t}\right) \tag{3}$$

$$q_t = \frac{k_2 {q_e}^2 t}{(1 + k_2 q_e t)} \tag{4}$$

where q_t (mg/g) is the amount of MB adsorbed at a time t (min) and q_e (mg/g) is the adsorption capacity of MCLB at equilibrium. k_1 (min^{-1}) represents pseudo-first-order and k_2 (g $mg^{-1}min^{-1}$) represents a pseudo-second-order rate. By plotting the graph between q_t

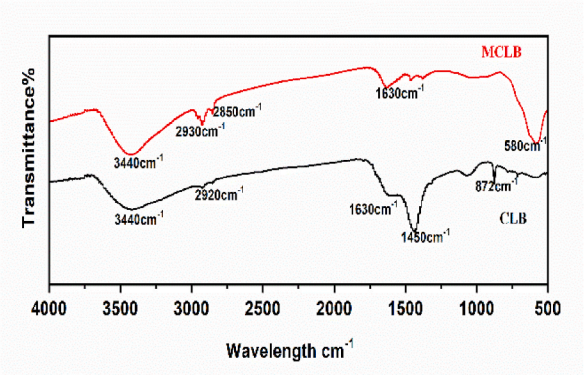

Fig. 2. FTIR spectra of CLB and MCLB.

vs t the values of k_1 and q_e can be derived with the help of Eq. (3). While the value of q_e and k_2 are obtained employing Eq. (4).

2.5. Adsorption isotherms

Adsorption isotherms can evaluate the capacity of an adsorbent and help understand the underlying physicochemical nature, which has practical applications [41]. For isotherm modeling Langmuir isotherm, Freundlich isotherm, and Temkin isotherm models non-linear fitting were used to analyze the equilibrium data obtained. The monolayer adsorption model also called the Langmuir isotherm model assumes that the energy of active sites on the adsorbent surface is uniform. It is considered that the adsorption is localized. No further adsorption can occur on an active site after a dye molecule has occupied it. Furthermore, the interactions between the dye molecules were disregarded. Equation (5) is used to obtain the equilibrium absorption capacity according to Langmuir isotherm [42]:

$$q_e = \frac{q_m \,.K.C_e}{1 + K_L \,.\ C_e} \tag{5}$$

where, K_L, is the Langmuir constant related to the affinity of the binding sites, L/mg; C_e, the MB concentration at absorption equilibrium, mg/L; q_m the maximal adsorption capacity, mg/g. The Langmuir isotherm parameters q_m and K_L were determined using a non-linear approach.

The Freundlich isotherm model is based on the fact that the surface energy of the adsorbent is uniform, but instead is heterogenous. This non-uniformity leads to the occupation of stronger binding sites first, and as the number of occupied sites rises, binding strength decreases. Equation (6) expresses the non-linear form of Freundlich adsorption isotherm [43]:

$$q_e = K_F.C_e^{\,1/n} \tag{6}$$

where K_F is the Freundlich adsorption capacity of the adsorbent, $L^{1/n}\ mg^{(1-1/n)}/g$; n is the surface heterogeneity factor, $n > 1$ [44].

The Freundlich isotherm parameters (K_F and n) were calculated by optimizing the correlation coefficients between the value of q_e calculated experimentally and theoretically applied in equation (6).

According to the Temkin isotherm model, with increasing coverage, the heat of adsorption of all molecules is reduced linearly. The resulting decrease in heat is caused by the adsorbent-adsorbate interactions, which are characterized by the factor of homogenous binding energy distribution. Equation (7) expresses the Temkin isotherm model [44]:

$$q_e = \frac{RT}{\beta_T} \,.\, ln\left(\alpha_T c_e\right) \tag{7}$$

where T is the adsorption temperature in K; R is the universal gas constant, 8.314 J/(mol K); α_T, the Temkin isotherm equilibrium binding constant is decided by maximum binding energies, L/mol; β_T, the Temkin isotherm constant; J/mol. Adsorption heat (J/mol) can be calculated as $q_a = \frac{RT}{\beta_T}$ [45].

3. Results and discussion

3.1. Physicochemical characteristics of MCLB

The amount of material remaining from the carbonization process (g) was used to calculate the carbonization yield;

$$CY\ (\%) = mass\ of\ biochar\ produced\ (g)\ /\ mass\ of\ biomass\ (g)\ X\ 100$$

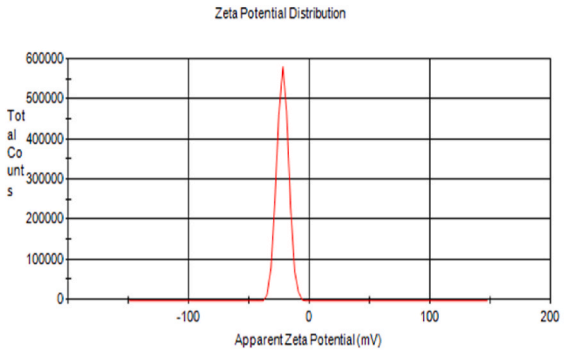

Fig. 3. Zeta potential distribution of MCLB.

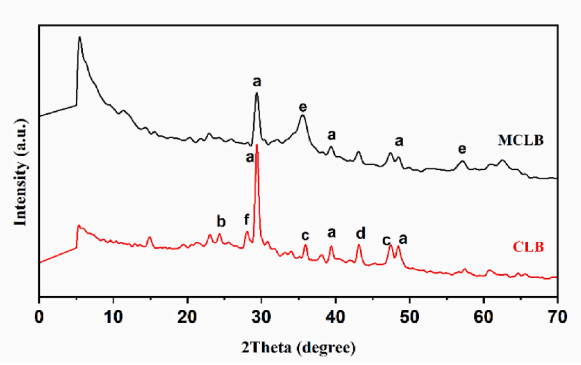

Fig. 4. XRD patterns for CLB and MCLB. Identified peaks include: a = SiO_2, b = Graphite, c = $CaCO_3$, d = MgO, e = Fe_2O_3, f = KCl.

$$Yield\ of\ MCLB\ (\%) = mass\ of\ MCLB\ (g)\ /\ mass\ of\ biochar\ (g)\ X\ \ 100$$

Product	% Yield
Citrus limetta biochar (CLB)	15.04
Magnetized *Citrus limetta* biochar (MCLB)	42.8

3.2. Characterizations of MCLB

3.2.1. Fourier transform IR spectra

The distribution of functional groups in the material was investigated using FTIR spectra from the obtained transmittance (vibrational) spectra. Similar spectra in Fig. 2 between the *Citrus limetta* biochar (CLB) and the magnetized biochar (MCLB) suggest similar functional groups. The spectra demonstrated the existence of many lignocellulosic material-specific bands, such as aromatic, hydroxyl, carbonyl, and alkene. The presence of a large absorption peak at 3440 cm^{-1} was attributed to the O–H stretching vibration of hydroxyl functional groups involving hydrogen bonding [46]. A lower intensity peak has been identified for aliphatic –CH stretching at 2920 cm^{-1} for biochar (CLB) which has been shifted to 2930 cm^{-1} in magnetized biochar (MCLB) [47].The peaks at 1630 cm^{-1},1450 cm^{-1} were indicative of C═C, and C–N stretching vibration respectively [42]. The aromatic structures are represented as the band at 872 cm^{-1}, which belongs to aromatic and furfural -C-H out-of-plane bending vibrations [42]. According to the analysis of the FTIR spectra of MCLB the peaks detected for unmodified biochar were suppressed, indicating that the surface modification obscured these functionalities. The presence of an additional peak at 580 cm^{-1} that is associated with Fe–O vibrations suggests that iron oxides have successfully modified on the surfaces [1].

3.2.2. Zeta potential

The negative zeta potential (−22 mV) of synthesized MCLB showed that it has a negatively charged surface Fig. 3. Increasing the pyrolysis temperature resulted in a decrease in the zeta potential of biochar, *i.e.* another explanation for the enhanced adsorption efficiency of MCLB is that the biochar generated at lower temperatures carried more negative surface charges than those synthesized at higher temperatures [5].

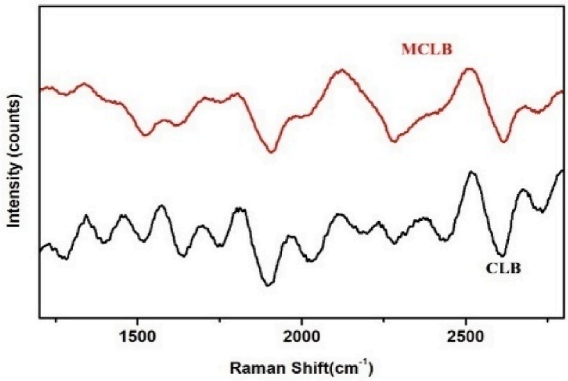

Fig. 5. Raman spectra of CLB and MCLB.

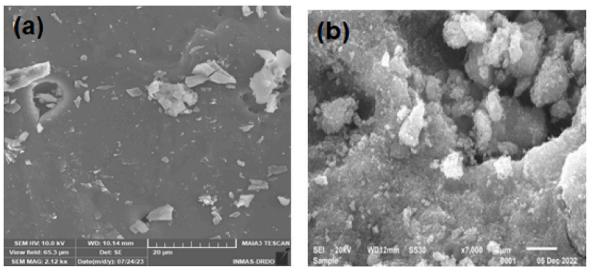

Fig. 6. SEM image of (a) CLB and (b) MCLB.

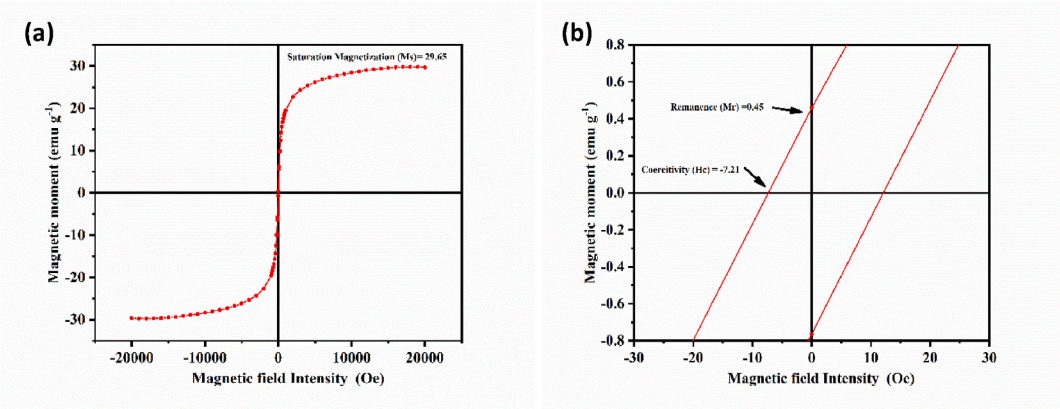

Fig. 7. (a) and (b): Magnetic hysteresis curve of MCLB.

3.2.3. X-ray diffraction (XRD)

X-ray diffraction (XRD) characterization technique was utilized to analyze the crystal structure of the magnetized biochar material MCLB. The XRD patterns of biochar (CLB) and magnetized biochar (MCLB) are represented in Fig. 4. In the XRD pattern for biochar (MCLB), there are some identifiable peaks of SiO_2 [13] and Fe_2O_3 [48]. However, there are SiO_2, $CaCO_3$ [49], KCl [50], MgO [51] and graphite [52] are all evident peaks in the XRD pattern for biochar (CLB) Fig. 4. These observations may suggest that the iron oxide component is in the non-crystalline amorphous phase. The XRD patterns of CLB and MCLB demonstrated that it was edging towards an amorphous-like structure while still having some crystal structure. The graphite peaks vanished in the MCLB due to the graphite phase changing to an amorphous phase during the magnetization process.

3.2.4. Raman spectra

Raman spectroscopy is an effective technique for investigating carbonaceous materials, particularly those sp^2 or nearly sp^2, including graphite, carbon nanotubes, and graphene. Raman spectra of MCLB and CLB are illustrated in Fig. 5. As shown in figure

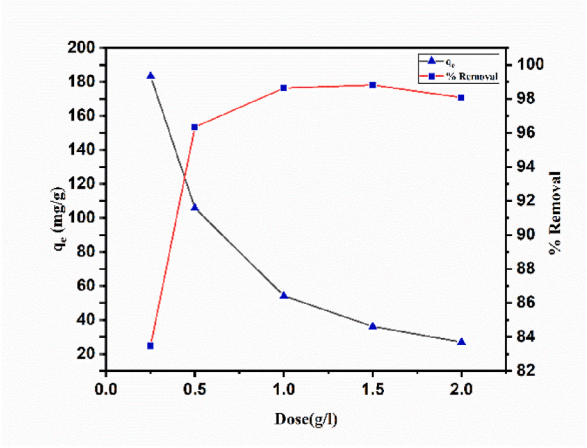

Fig. 8. The effect of MCLB dosage (0.25–2.0) g/L on MB removal at initial MB concentration of 50 mg/L at unadjusted pH(pH = 6.8) and contact time (3hr).

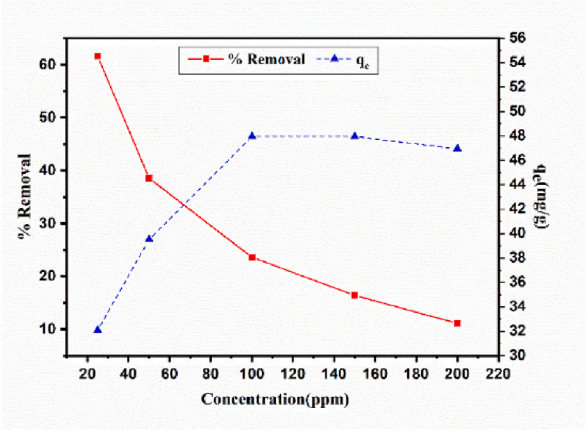

Fig. 9. Effect of initial MB concentration on % Removal and adsorption capacity of MCLB at (25–200) mg/L range MB concentration, 0.5 g/L adsorbent dose, and unadjusted pH (pH ~ 6.8).

MCLB graphitic planes are absent [53]. Biochar when carbonized at low temperatures shows similar Raman spectra with no distinguishable peaks [13].

3.2.5. Scanning electron microscope (SEM)

The SEM image of MCLB was found to be asymmetrical and irregular layered particles Fig. 6 (b) SEM images of MCLB composite surface revealed the presence of distributed Fe_2O_3, implying successful attachment of iron oxide onto biochar material. Whereas, Fig. 6 (a) shows that the CLB had a smooth surface and a porous structure [34]. According to SEM images shown in Fig. 6(b), MCLB has a fluffy, disorganized, coarse, and uneven surface with no evident pore structure [1].

3.2.6. Vibrating- sample magnetometer (VSM)

The dispersed Fe_2O_3 onto the biochar surface introduces the magnetism onto biochar (MCLB). To analyze the magnetic strength of synthesized MCLB, the hysteresis loop of MCLB was determined at room temperature (298 K) with a vibrating-sample magnetometer (VSM) Fig. 7 [54].The negligible value of coercivity ($H_c = -7.21$) and remanence ($M_r = 0.45$) resulted that MCLB possesses superparamagnetic behavior. The findings demonstrate that the hysteresis loop exhibits superparamagnetic properties and is symmetric about the origin. The saturation magnetization value (M_s) for MCLB is 29.65 emu $g^{-1}$and It was possible to completely separate it from the aqueous solution by using an external magnet [55].

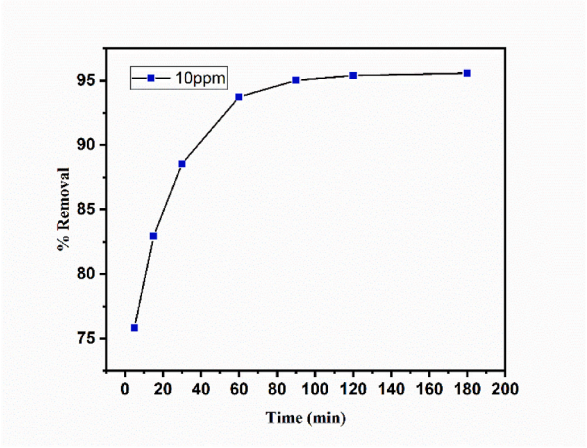

Fig. 10. Results for effect of contact time on MB removal at 10 mg/L, absorbent dose 1 g/L and pH = 6.8.

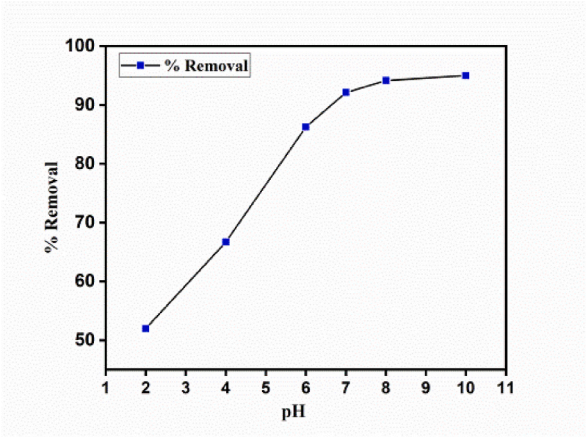

Fig. 11. Effect of pH on MB adsorption by MCLB at 20 mL MB solution (50 mg/L), pH = 2–10, adsorbent dose = 0.5 g/L, contact time (3hr).

4. Adsorption optimization and adsorption isotherm

4.1. Effects of MCLB dosage

The adsorption capacity of MB onto MCLB is significantly affected by the dosage of MCLB used. A batch of 20 mL of MB 50 mg/L solution was treated with a variable dosage of MCLB adsorbent (0.25–2.0) g/L to determine the effects of different adsorbent doses. Fig. 8 depicts the varying dosage effect of MCLB on MB removal efficiency and MCLB adsorption capacity. The obtained result indicates that the removal efficiency increased as the MCLB dose was raised from 0.25 g/L to 1 g/L. Almost 98 % removal of MB was observed at 1 g/L dosage of MCLB. It has been observed that the number of active sites increases up to a certain optimal level [56]. However, when the MCLB dose was increased, the adsorption capacity of MCLB was reduced. This might be because there were fewer MB molecules per unit of adsorbent or lesser active adsorption sites created as a consequence of the agglomeration of the adsorbent [1]. With larger dosages, MCLB loses active binding sites and surface area, which results in a reduction in adsorption capacity. Thus, the most optimal dose of MCLB for the effective adsorption of MB is found to be 1 g/L.

4.2. Effect of initial concentration

To examine the effect of initial MB concentration on the adsorption capacity of MCLB, the experiments were performed at (25–200) mg/L concentration range with 0.5 g/L dose of MCLB. The pH was unadjusted (pH ~ 6.8) and the contact time was given as 3 h to reach equilibrium. It has resulted that, at an initial lower concentration of MB, the adsorbent MCLB showed a good adsorption performance Fig. 9. As there was a high amount of vacant sites available in comparison to the MB concentration [57]. As the initial MB concentration of MB increased above 100 mg/L, the adsorption capacity tends to decrease. This may occur as a result of MB molecules accumulating, which could impact the binding rate at which MB adheres to the MCLB surface. More active sites were thus occupied on

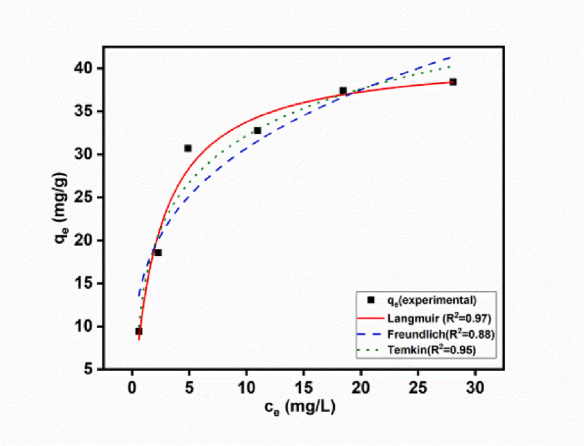

Fig. 12. Non-linear Langmuir, Freundlich, and Temkin isotherm fitting curves for MB adsorption onto MCLB.

Table 2
Calculated results of adsorption isotherms.

Isotherm models	Isotherm Parameters			R^2
Langmuir	q_m	K_L	R_L	0.97
	41.57	0.43	3.73×10^{-2}	
Freundlich	n_F	K_F	1/n	0.90
	3.57	15.82	0.28	
Temkin	β_T	α_T		0.96
	7.84	6.04		

the external surface of the MCLB, which caused competitive absorption and a decrease in MB adsorption [46].

4.3. Effect of contact time

Researchers have extensively investigated the fact that neutral pH or mildly basic conditions are ideal for MB adsorption [1,40]. For a 10 mg/L concentration and a dose of 1 g/L of MCLB at an uncorrected pH (pH = 6.8), at predetermined intervals (0–180 min), the effect of contact time on the % removal of MB was examined. The findings are displayed in Fig. 10. Suggesting that adsorption occurs predominantly on the MCLB surface during the initial phase, the maximum adsorption rate (up to 95 % removal) was acquired during the 90-min contact time. Therefore, a contact time of 90 min was deemed to be the optimal duration for the adsorption process to attain equilibrium. These findings demonstrate the normal course of the adsorption process, which culminates when the maximal adsorption capacity is reached and the accessible sites are entirely filled with MB molecules over an increasing period [58]. The percentage removal remained almost constant after this point until the adsorption equilibrium was attained at around 180 min.

4.4. Effect of pH value

The pH of the solution affects the chemical nature of the adsorbate and the charge density of the adsorbent surface. Hence, it was determined under what pH conditions the impact of solution pH on the effectiveness of MB removal (2−10). The outcomes shown in Fig. 11 illustrate that when the pH of the MB solution was raised from acidic to neutral; the removal efficiency of MB progressively arose and then stayed almost constant as the pH was raised further. A dosage of 0.1 g/L of MCLB for 50 mg/L of MB solution was used to achieve the highest level of adsorption at a pH of 8. The reduced MB adsorption in the lower pH range also shows the possibility for neutral or weaker charges to accumulate on the surface of MCLB, which would diminish the electrostatic pull for the MB to adsorb onto MCLB. However, at neutral pH and in basic media, the creation of an electric double layer alters its polarity, boosting MB adsorption [59].

4.5. Adsorption isotherm

The adsorption isotherms of MB adsorption onto MCLB are shown in Fig. 12. The significant isotherm parameters for the observed adsorption data plotted between c_e vs q_e are presented in Table 2 using the non-linear Langmuir isotherm, Freundlich isotherm, and Temkin isotherm models. Once the system achieved an equilibrium state with equilibrium concentration c_e (mg/L) and equilibrium adsorption capacity q_e (mg/g), the adsorption capacity related to active sites on the MCLB surface could be investigated.). It is possible to draw the conclusion that since the Langmuir isotherm model has the highest correlation coefficient value (R^2 = 0.97), it best

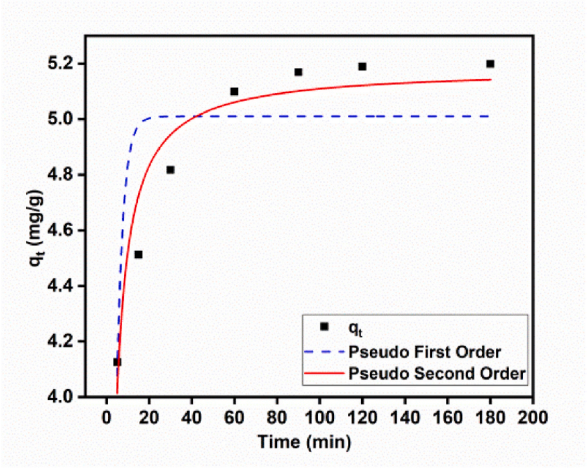

Fig. 13. Kinetic adsorption non-linear fitting for MB adsorption onto MCLB.

Table 3
Calculated results for non-linear pseudo-first order and pseudo-second order kinetic models for MCLB.

Kinetic model	$q_{e\ expeimental}$ (mg/g)	Parameters		R^2
Pseudo-first order	5.19 mg/g	$q_{e\ 1}$(mg/g)	k_1(1/min)	0.65
		5.01	0.33	
Pseudo-second order		$q_{e\ 2}$(mg/g)	k_2(g/mg min)	0.91
		5.18	0.13	

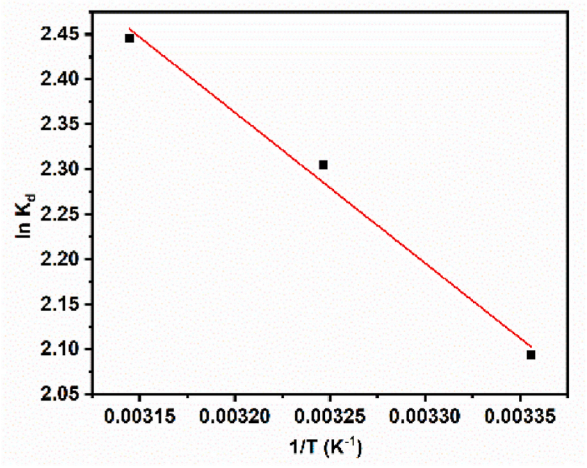

Fig. 14. MB adsorption onto MCLB at 298, 308, and 318 K temperatures. 20 mL MB solution (20 mg/L), pH unadjusted, adsorbent dose = 0.5 g/L, contact time (3hr).

explains how adsorption works. This illustrated MB adsorbed on MCLB following monolayer adsorption mechanism with a good maximum adsorption capacity of q_{max} = 41.57 (mg/g) for MB (c_o = 60 mg/L, pH ~ 6.8, T = 273K).

The Langmuir isotherm model suggests that a separation parameter, R_L (dimensionless) expressed in equation (8), can be used to analyze the adsorption process. Which is used to indicate whether or not the adsorption process is favorable. favorable when ($0<R_L<1$), unfavorable when ($R_L \geq 1$), and irreversible when ($R_L = 0$) [60].

$$R_L = 1 / (1 + K_L c_o) \tag{8}$$

where, K_L is the Langmuir constant and c_o is the initial MB concentration. The R_L value calculated was <1 (R_L 3.73 × 10^{-2}), which resulted that the adsorption of MB molecules by MCLB is favorable [44]. The observed 1/n value in the Freundlich model was less than 1, which also shows good adsorption [1]. According to the Temkin isotherm, a positive β_T value demonstrates that the adsorption

Table 4
Thermodynamics parameters for MB adsorption onto MCLB.

Temperature (K)	ΔG^0 (kJ/mol)	ΔH^0 (kJ/mol)	ΔS^0 (J/K.mol)
298	−5.18	13.89	64.11
308	−5.90		
318	−6.46		

process is exothermic [61].

4.6. Adsorption kinetics

The outcomes of the experiment were analyzed using non-linear pseudo-first-order and pseudo-second-order kinetics models; graphs are presented in Fig. 13, and Table 3 summarizes the obtained parameters. As can be observed from Fig. 13, The non-linear pseudo-second-order model expressed better suitability for removal of MB dye and their fitting results were much closer to experimental data (at 10 mg/L initial concentration of MB, 0.5 g/L dose of MCLB, pH ~ 6.8, T = 273K). Also, the calculated value of adsorption capacity ($q_{e\ cal}$ = 5.18 mg/g) is closer to the experimental value ($q_{e\ exp}$ = 5.19 mg/g). The existence of electrostatic interactions between adsorbent and adsorbate, ion exchange, and the formation of a complex of MB and MCLB is indicated by the good fitting of the pseudo-second-order kinetics model [10]. When the rate constant k_2 for the pseudo-second-order kinetic model is larger it takes less time for the adsorption process to reach equilibrium [62].

4.7. Effects of temperature and adsorption thermodynamics

Adsorption thermodynamics was carried out at the optimal values of batch solutions at an equilibrium contact time of 3 h, with the solution pH unadjusted (pH ~ 6.8), and the adsorbent dosage of 0.5 g/L. The equilibrium coefficient, K_d (mL/g) was calculated at temperatures 298, 308, and 318 K respectively, q_e is the equilibrium adsorption capacity (mg/g) and c_e is the equilibrium concentration of MB (mg/L). T is the system temperature (K) and R is the universal gas constant (8.314 J/mol K).

The Van't Hoff plot is shown in the linearized form in Fig. (14), to investigate changes in standard enthalpy ΔH^0 (kJ/mol) and standard entropy ΔS^0 (J/K.mol). Using the following equations, the change in Gibbs free energy ΔG^0 (kJ/mol) is then determined [63].

$$K_d = \frac{q_e}{c_e} \tag{9}$$

$$ln\ K_d = \frac{\Delta S}{R} \tag{10}$$

$$\Delta G = \Delta H - T\Delta S \tag{11}$$

Table 4 displays the calculated thermodynamics parameters. While the positive ΔS value (64.11 J/K mol) suggests that the randomization of the adsorbent-adsorbate interface rises during the fixation of MB molecules on the active sites of MCLB, the positive ΔH value (13.89 kJ/mol) implies an endothermic adsorption process [64]. The feasibility of MB adsorption onto MCLB is demonstrated by negative G values (−5.18 to −6.46 kJ/mol), which correspond to a physisorption process [1].

5. Conclusion

The major objective of the current study was to use value-added by-products (Citrus limetta peels) to conserve the environment and make beneficial use of this resource. The MCLB, a magnetic biochar adsorbent facilely prepared from fruit peel waste (Citrus limetta), showed an excellent MB adsorption capacity of 41.57 mg/g. The Pseudo second-order kinetics and Langmuir adsorption isotherm model's non-linear fitting were applied to represent the most effective isotherm models. As a result, under ideal conditions (i.e., solution pH = 8, contact time of 90 min, and adsorbent dose of 1 g/L), the magnetized biochar adsorbent made from food waste (MCLB) showed good ability to extract MB dye from aqueous solutions. The thermodynamic study demonstrated the spontaneous and endothermic nature of MB adsorption on MCLB. The hysteresis loop of MCLB obtained from VSM showed its superparamagnetic nature with saturation magnetization (Ms) value 29.65 emu g-1. The magnetic property makes the adsorbent easily magnetically separable after the adsorption process. Our research showed that MCLB could substitute adsorbent material for future large-scale industrial wastewater treatment.

CRediT authorship contribution statement

Ayushi Mishra: Data curation, Formal analysis, Writing – original draft, Writing – review & editing. **Himanshu Ojha:** Funding acquisition, Investigation, Methodology, Resources. **Jyoti Pandey:** Resources, Supervision. **Anjani Kumar Tiwari:** Investigation, Resources, Validation. **Mallika Pathak:** Conceptualization, Formal analysis, Supervision, Writing – review & editing.

Declaration of competing interest

The authors declare that they have no known competing financial interests personal relationships that could have appeared to influence the work reported in this paper.

Acknowledgements

All authors are sincerely thankful to Dr. Anil K Mishra, Scientist “G”, Director of the Institute of Nuclear Medicine and Allied Sciences (INMAS) for supporting this research work. The authors are grateful to Dr. Amit Tyagi Sc “F” (INMAS) for SEM facility, Babasaheb Bhimrao Ambedkar University, Lucknow, and Miranda House College, University of Delhi, Delhi. We are thankful to Miss Lajpreet Kaur (CSIR-SRF) for her constant support and guidance.

References

[1] P. Zhang, D. O’Connor, Y. Wang, L. Jiang, T. Xia, L. Wang, D.C.W. Tsang, Y.S. Ok, D. Hou, A green biochar/iron oxide composite for methylene blue removal, J. Hazard Mater. 384 (2020), 121286, https://doi.org/10.1016/j.jhazmat.2019.121286.
[2] I. Khan, K. Saeed, I. Zekker, B. Zhang, A.H. Hendi, A. Ahmad, S. Ahmad, N. Zada, H. Ahmad, L.A. Shah, T. Shah, I. Khan, Review on Methylene Blue: its Properties, Uses, Toxicity and Photodegradation, Water, (Switzerland, 2022, p. 14, https://doi.org/10.3390/w14020242.
[3] P. Grau, Textile industry wastewaters treatment, Water Sci. Technol. 24 (1991) 97–103, https://doi.org/10.2166/wst.1991.0015.
[4] V.K. Garg, M. Amita, R. Kumar, R. Gupta, Basic dye (methylene blue) removal from simulated wastewater by adsorption using Indian Rosewood sawdust: a timber industry waste, Dyes Pigments 63 (2004) 243–250, https://doi.org/10.1016/j.dyepig.2004.03.005.
[5] Y. Zhu, B. Yi, Q. Yuan, Y. Wu, M. Wang, S. Yan, Removal of methylene blue from aqueous solution by cattle manure-derived low temperature biochar, RSC Adv. 8 (2018) 19917–19929, https://doi.org/10.1039/c8ra03018a.
[6] J. Bu, L. Yuan, N. Zhang, D. Liu, Y. Meng, X. Peng, High-efficiency adsorption of methylene blue dye from wastewater by a thiosemicarbazide functionalized graphene oxide composite, Diam. Relat. Mater. 101 (2020), https://doi.org/10.1016/j.diamond.2019.107604.
[7] Z. Chen, M. Hu, X. Zhu, D. Guo, S. Liu, Z. Hu, B. Xiao, J. Wang, M. Laghari, Characteristics and kinetic study on pyrolysis of five lignocellulosic biomass via thermogravimetric analysis, Bioresour. Technol. 192 (2015) 441–450, https://doi.org/10.1016/j.biortech.2015.05.062.
[8] D. Mohan, A. Sarswat, Y.S. Ok, C.U. Pittman, Organic and inorganic contaminants removal from water with biochar, a renewable, low cost and sustainable adsorbent - a critical review, Bioresour. Technol. 160 (2014) 191–202, https://doi.org/10.1016/j.biortech.2014.01.120.
[9] B. Chen, Z. Chen, S. Lv, A novel magnetic biochar efficiently sorbs organic pollutants and phosphate, Bioresour. Technol. 102 (2011) 716–723, https://doi.org/10.1016/j.biortech.2010.08.067.
[10] L. Zhou, Y. Liu, S. Liu, Y. Yin, G. Zeng, X. Tan, X. Hu, X. Hu, L. Jiang, Y. Ding, S. Liu, X. Huang, Investigation of the adsorption-reduction mechanisms of hexavalent chromium by ramie biochars of different pyrolytic temperatures, Bioresour. Technol. 218 (2016) 351–359, https://doi.org/10.1016/j.biortech.2016.06.102.
[11] M. Rafatullah, O. Sulaiman, R. Hashim, A. Ahmad, Adsorption of methylene blue on low-cost adsorbents: a review, J. Hazard Mater. 177 (2010) 70–80, https://doi.org/10.1016/j.jhazmat.2009.12.047.
[12] C. Liu, W. Wang, R. Wu, Y. Liu, X. Lin, H. Kan, Y. Zheng, Preparation of acid- and alkali-modified biochar for removal of methylene blue pigment, ACS Omega 5 (2020) 30906–30922, https://doi.org/10.1021/acsomega.0c03688.
[13] N.G. Gonzalez-Canche, J.G. Carrillo, B. Escobar-Morales, I. Salgado-Tránsito, N. Pacheco, S.C. Pech-Cohuo, M.I. Peña-Cruz, Physicochemical and optical characterization of citrus aurantium derived biochar for solar absorber applications, Materials 14 (2021), https://doi.org/10.3390/ma14164756.
[14] N. Mahato, K. Sharma, M. Sinha, A. Dhyani, B. Pathak, H. Jang, S. Park, S. Pashikanti, S. Cho, Biotransformation of Citrus Waste-I: Production of Biofuel and Valuable Compounds by Fermentation, 2021, https://doi.org/10.3390/pr9020220.
[15] J. Banerjee, R. Singh, R. Vijayaraghavan, D. MacFarlane, A.F. Patti, A. Arora, Bioactives from fruit processing wastes: green approaches to valuable chemicals, Food Chem. 225 (2017) 10–22, https://doi.org/10.1016/j.foodchem.2016.12.093.
[16] NAAS, Saving the harvest: reducing the food loss and waste, Policy Brief 5 (2019) 10.
[17] H. Kumar, K. Bhardwaj, R. Sharma, E. Nepovimova, K. Kuča, D.S. Dhanjal, R. Verma, P. Bhardwaj, S. Sharma, D. Kumar, Fruit and vegetable peels: utilization of high value horticultural waste in novel industrial applications, Molecules 25 (2020), https://doi.org/10.3390/molecules25122812.
[18] M. Wadhwa, S.P.M. Bakshi, Utilization of Fruit and Vegetable Wastes as Livestock Feed and as Substrates for Generation of Other Value-Added Products, 2013.
[19] H. Everitt, P. van der Werf, J.A. Seabrook, A. Wray, J.A. Gilliland, The quantity and composition of household food waste during the COVID-19 pandemic: a direct measurement study in Canada, Socioecon Plann Sci 82 (2022), 101110, https://doi.org/10.1016/j.seps.2021.101110.
[20] I. Boudraa, S.U. Odabasi, M. Bareera, H. Ayadi, B. Kebabi, H. Buyukgungor, Magnetization of a biochar derived from orange peel and its application for the removal of crystal violet, Applied Environmental Research 44 (2022) 88–100, https://doi.org/10.35762/AER.2022.44.3.7.
[21] M.B. Ahmed, J.L. Zhou, H.H. Ngo, W. Guo, M. Chen, Progress in the preparation and application of modified biochar for improved contaminant removal from water and wastewater, Bioresour. Technol. 214 (2016) 836–851, https://doi.org/10.1016/j.biortech.2016.05.057.
[22] A.R. Lucaci, D. Bulgariu, I. Ahmad, G. Lisa, A.M. Mocanu, L. Bulgariu, Potential use of biochar from variouswaste biomass as biosorbent in Co(II) removal processes, Water (Switzerland) (2019) 11, https://doi.org/10.3390/w11081565.
[23] J. Wu, J. Yang, P. Feng, G. Huang, C. Xu, B. Lin, High-efficiency removal of dyes from wastewater by fully recycling litchi peel biochar, Chemosphere 246 (2020), 125734, https://doi.org/10.1016/j.chemosphere.2019.125734.
[24] K. Bouhadjra, W. Lemlikchi, A. Ferhati, S. Mignard, Enhancing removal efficiency of anionic dye (Cibacron blue) using waste potato peels powder, Sci. Rep. (2021) 1–10, https://doi.org/10.1038/s41598-020-79069-5.
[25] A.H. Jawad, A. Saud Abdulhameed, L.D. Wilson, S.S.A. Syed-Hassan, Z.A. Alothman, M. Rizwan Khan, High surface area and mesoporous activated carbon from KOH-activated dragon fruit peels for methylene blue dye adsorption: optimization and mechanism study, Chin. J. Chem. Eng. 32 (2021) 281–290, https://doi.org/10.1016/j.cjche.2020.09.070.
[26] H.K. Yağmur, İ. Kaya, Synthesis and characterization of magnetic ZnCl2-activated carbon produced from coconut shell for the adsorption of methylene blue, J. Mol. Struct. 1232 (2021), https://doi.org/10.1016/j.molstruc.2021.130071.
[27] O.S. Bayomie, H. Kandeel, T. Shoeib, H. Yang, N. Youssef, M.M.H. El-Sayed, Novel approach for effective removal of methylene blue dye from water using fava bean peel waste, Sci. Rep. 10 (2020) 1–10, https://doi.org/10.1038/s41598-020-64727-5.
[28] T.H. Do, V.T. Nguyen, N.Q. Dung, M.N. Chu, D. Van Kiet, T.T.K. Ngan, L. Van Tan, Study on methylene blue adsorption of activated carbon made from Moringa oleifera leaf, Mater. Today Proc. 38 (2020) 3405–3413, https://doi.org/10.1016/j.matpr.2020.10.834.
[29] P.N.Y. Yek, W. Peng, C.C. Wong, R.K. Liew, Y.L. Ho, W.A. Wan Mahari, E. Azwar, T.Q. Yuan, M. Tabatabaei, M. Aghbashlo, C. Sonne, S.S. Lam, Engineered biochar via microwave CO2 and steam pyrolysis to treat carcinogenic Congo red dye, J. Hazard Mater. 395 (2020), https://doi.org/10.1016/j.jhazmat.2020.122636.
[30] E. Misran, O. Bani, E.M. Situmeang, A.S. Purba, Banana stem based activated carbon as a low-cost adsorbent for methylene blue removal: isotherm, kinetics, and reusability, Alex. Eng. J. 61 (2022) 1946–1955, https://doi.org/10.1016/j.aej.2021.07.022.

[31] L.Q. Xie, X.Y. Jiang, J.G. Yu, A novel low-cost bio-sorbent prepared from crisp persimmon peel by low-temperature pyrolysis for adsorption of organic dyes, Molecules 27 (2022), https://doi.org/10.3390/molecules27165160.

[32] S. Vigneshwaran, P. Sirajudheen, P. Karthikeyan, S. Meenakshi, Fabrication of sulfur-doped biochar derived from tapioca peel waste with superior adsorption performance for the removal of Malachite green and Rhodamine B dyes, Surface. Interfac. 23 (2021), 100920, https://doi.org/10.1016/j.surfin.2020.100920.

[33] M.U. Dao, H.S. Le, H.Y. Hoang, V.A. Tran, V.D. Doan, T.T.N. Le, A. Sirotkin, V.T. Le, Natural core-shell structure activated carbon beads derived from Litsea glutinosa seeds for removal of methylene blue: facile preparation, characterization, and adsorption properties, Environ. Res. 198 (2021), 110481, https://doi.org/10.1016/j.envres.2020.110481.

[34] V.H. Nguyen, H.T. Van, V.Q. Nguyen, X. Van Dam, L.P. Hoang, L.T. Ha, L.T. Ha, Magnetic Fe3O4Nanoparticle biochar derived from pomelo peel for reactive red 21 adsorption from aqueous solution, J. Chem. 2020 (2020), https://doi.org/10.1155/2020/3080612.

[35] H. Park, J. Kim, Y.G. Lee, K. Chon, Enhanced adsorptive removal of dyes using Mandarin peel biochars via chemical activation with nh4cl and zncl2, Water (Switzerland) (2021) 13, https://doi.org/10.3390/w13111495.

[36] P.M. Thabede, N.D. Shooto, E.B. Naidoo, Removal of methylene blue dye and lead ions from aqueous solution using activated carbon from black cumin seeds, S. Afr. J. Chem. Eng. 33 (2020) 39–50, https://doi.org/10.1016/j.sajce.2020.04.002.

[37] R.T. Kapoor, M. Rafatullah, A.M. Aljuwayid, M.A. Habila, S.M. Wabaidur, M. Alam, Removal of patent blue dye using ananas comosus-derived biochar: equilibrium, kinetics, and phytotoxicity studies, Separations 9 (2022), https://doi.org/10.3390/separations9120426.

[38] P. Boakye, H.N. Tran, D.S. Lee, S.H. Woo, Effect of water washing pretreatment on property and adsorption capacity of macroalgae-derived biochar, J. Environ. Manag. 233 (2019) 165–174, https://doi.org/10.1016/j.jenvman.2018.12.031.

[39] L.C.A. Oliveira, R.V.R.A. Rios, J.D. Fabris, V. Garg, K. Sapag, R.M. Lago, Activated carbon/iron oxide magnetic composites for the adsorption of contaminants in water, Carbon N Y 40 (2002) 2177–2183, https://doi.org/10.1016/S0008-6223(02)00076-3.

[40] Y. Mu, H. Du, W. He, H. Ma, Functionalized mesoporous magnetic biochar for methylene blue removal: performance assessment and mechanism exploration, Diam. Relat. Mater. 121 (2022), https://doi.org/10.1016/j.diamond.2021.108795.

[41] A.J. Rahman, H. Ojha, A. Pandey, S. Kumar, R. Singhal, A. Datta, B.K. Singh, Kinetic, isotherm and thermodynamic adsorption studies of organophosphorus compound (phosmet) on reduced graphene oxide, Diam. Relat. Mater. 127 (2022), 109191, https://doi.org/10.1016/j.diamond.2022.109191.

[42] W. Astuti, T. Sulistyaningsih, E. Kusumastuti, G.Y.R.S. Thomas, R.Y. Kusnadi, Thermal conversion of pineapple crown leaf waste to magnetized activated carbon for dye removal, Bioresour. Technol. 287 (2019), 121426, https://doi.org/10.1016/j.biortech.2019.121426.

[43] E. Altıntıg, H. Altundag, M. Tuzen, A. Sarı, A. Sarı, Effective removal of methylene blue from aqueous solutions using magnetic loaded activated carbon as novel adsorbent, Chem. Eng. Res. Des. 122 (2017) 151–163, https://doi.org/10.1016/j.cherd.2017.03.035.

[44] X. Zhang, L. Lv, Y. Qin, M. Xu, X. Jia, Z. Chen, Removal of aqueous Cr(VI) by a magnetic biochar derived from Melia azedarach wood, Bioresour. Technol. 256 (2018) 1–10, https://doi.org/10.1016/j.biortech.2018.01.145.

[45] D. A.O, Langmuir, Freundlich, Temkin and dubinin–radushkevich isotherms studies of equilibrium sorption of Zn 2+ unto phosphoric acid modified rice husk, IOSR J. Appl. Chem. 3 (2012) 38–45, https://doi.org/10.9790/5736-0313845.

[46] M.J. Ahmed, P.U. Okoye, E.H. Hummadi, B.H. Hameed, High-performance porous biochar from the pyrolysis of natural and renewable seaweed (Gelidiella acerosa) and its application for the adsorption of methylene blue, Bioresour. Technol. 278 (2019) 159–164, https://doi.org/10.1016/j.biortech.2019.01.054.

[47] A. Shakya, A. Núñez-Delgado, T. Agarwal, Biochar synthesis from sweet lime peel for hexavalent chromium remediation from aqueous solution, J. Environ. Manag. 251 (2019), https://doi.org/10.1016/j.jenvman.2019.109570.

[48] B.P. Singh, A. Kumar, H.I. Areizaga-Martinez, C.A. Vega-Olivencia, M.S. Tomar, Synthesis, characterization, and electrocatalytic ability of γ-Fe2O3 nanoparticles for sensing acetaminophen, Indian J. Pure Appl. Phys. 55 (2017) 722–728.

[49] F. Dehghani, A. Kalantariasl, R. Saboori, S. Sabbaghi, K. Peyvandi, Performance of carbonate calcium nanoparticles as filtration loss control agent of water-based drilling fluid, SN Appl. Sci. 1 (2019), https://doi.org/10.1007/s42452-019-1446-8.

[50] S.S. Sahoo, V.K. Vijay, R. Chandra, H. Kumar, Production and characterization of biochar produced from slow pyrolysis of pigeon pea stalk and bamboo, Cleaner Engineering and Technology 3 (2021), 100101, https://doi.org/10.1016/j.clet.2021.100101.

[51] A. Almontasser, A. Parveen, A. Azam, Synthesis, characterization and antibacterial activity of magnesium oxide (MgO) nanoparticles, IOP Conf. Ser. Mater. Sci. Eng. 577 (2019), https://doi.org/10.1088/1757-899X/577/1/012051.

[52] Q.T. Ain, S.H. Haq, A. Alshammari, M.A. Al-Mutlaq, M.N. Anjum, The systemic effect of PEG-nGO-induced oxidative stress in vivo in a rodent model, Beilstein J. Nanotechnol. 10 (2019) 901–911, https://doi.org/10.3762/BJNANO.10.91.

[53] A.C. Ferrari, Raman spectroscopy of graphene and graphite: disorder, electron-phonon coupling, doping and nonadiabatic effects, Solid State Commun. 143 (2007) 47–57, https://doi.org/10.1016/j.ssc.2007.03.052.

[54] J. Wang, M. Zhang, Adsorption characteristics and mechanism of bisphenol a by magnetic biochar, Int. J. Environ. Res. Publ. Health 17 (2020), https://doi.org/10.3390/ijerph17031075.

[55] X. Rong, M. Xie, L. Kong, V. Natarajan, L. Ma, J. Zhan, The magnetic biochar derived from banana peels as a persulfate activator for organic contaminants degradation, Chem. Eng. J. 372 (2019) 294–303, https://doi.org/10.1016/j.cej.2019.04.135.

[56] P. Zhang, I. Lo, D. O'Connor, S. Pehkonen, H. Cheng, D. Hou, High efficiency removal of methylene blue using SDS surface-modified ZnFe2O4 nanoparticles, J. Colloid Interface Sci. 508 (2017) 39–48, https://doi.org/10.1016/j.jcis.2017.08.025.

[57] D.K. Mahmoud, M.A.M. Salleh, W.A.W.A. Karim, A. Idris, Z.Z. Abidin, Batch adsorption of basic dye using acid treated kenaf fibre char: equilibrium, kinetic and thermodynamic studies, Chem. Eng. J. 181–182 (2012) 449–457, https://doi.org/10.1016/j.cej.2011.11.116.

[58] L. Ai, C. Zhang, F. Liao, Y. Wang, M. Li, L. Meng, J. Jiang, Removal of methylene blue from aqueous solution with magnetite loaded multi-wall carbon nanotube: kinetic, isotherm and mechanism analysis, J. Hazard Mater. 198 (2011), https://doi.org/10.1016/j.jhazmat.2011.10.041.

[59] X. Han, L. Chu, S. Liu, T. Chen, C. Ding, J. Yan, L. Cui, G. Quan, Removal of methylene blue from aqueous solution using porous biochar obtained by KOH activation of peanut shell biochar, Bioresources 10 (2015) 2836–2849, https://doi.org/10.15376/biores.10.2.2836-2849.

[60] M.A. Al-Ghouti, D.A. Da'ana, Guidelines for the use and interpretation of adsorption isotherm models: a review, J. Hazard Mater. 393 (2020), 122383, https://doi.org/10.1016/j.jhazmat.2020.122383.

[61] Z. Zhang, Z. Zhu, B. Shen, L. Liu, Insights into biochar and hydrochar production and applications: a review, Energy 171 (2019) 581–598, https://doi.org/10.1016/j.energy.2019.01.035.

[62] A. Shakya, A. Núñez-Delgado, T. Agarwal, Biochar synthesis from sweet lime peel for hexavalent chromium remediation from aqueous solution, J. Environ. Manag. 251 (2019), https://doi.org/10.1016/j.jenvman.2019.109570.

[63] Z. Chen, J. Zhang, J. Fu, M. Wang, X. Wang, R. Han, Q. Xu, Adsorption of methylene blue onto poly(cyclotriphosphazene-co-4,4'-sulfonyldiphenol) nanotubes: kinetics, isotherm and thermodynamics analysis, J. Hazard Mater. 273 (2014) 263–271, https://doi.org/10.1016/j.jhazmat.2014.03.053.

[64] T. Ai, X. Jiang, Q. Liu, L. Lv, H. Wu, Daptomycin adsorption on magnetic ultra-fine wood-based biochars from water: kinetics, isotherms, and mechanism studies, Bioresour. Technol. 273 (2019) 8–15, https://doi.org/10.1016/j.biortech.2018.10.039.